



Evolution of the LiFePO₄ positive electrode interface along cycling monitored by MAS NMR

Marine Cuisinier ^a, Nicolas Dupré ^{a,*}, Jean-Frédéric Martin ^{a,b}, Ryoji Kanno ^b, Dominique Guyomard ^a

^a Institut des Matériaux Jean Rouxel (IMN), CNRS UMR 6502, Université de Nantes, 2 rue de la Houssinière, BP32229, 44322 Nantes cedex 3, France

^b Department of Electronic Chemistry, Interdisciplinary Graduate School of Science and Engineering, Tokyo Institute of Technology, Midori, Yokohama 226-8502, Japan

HIGHLIGHTS

- Quantitative ⁷Li, ¹H and ¹⁹F NMR allow describing the interphase structure.
- Change of composition of interphase according to the potential.
- Accumulation of lithiated products at the positive surface along cycling.
- Interphasial species do not lead to the blocking of charge transfer.

ARTICLE INFO

Article history:

Received 23 May 2012

Received in revised form

26 July 2012

Accepted 22 August 2012

Available online 4 October 2012

Keywords:

Lithium batteries

Positive electrode

Interface

NMR

ABSTRACT

Decreasing particle size ensures a good accessibility of LiFePO₄ to lithium ions and electrons and allows reaching the theoretical capacity and achieving high cycling rates. It nevertheless leads to an increase of the surface area and thus a subsequent amplification of the parasitic reactions at the interface between active material surface and electrolyte. The formation and evolution of the interphase on the surface of LiFePO₄ may affect strongly its electrochemical performance. This work aims at monitoring the interphase forming on LiFePO₄ upon its operation in a lithium battery, and correlating its evolution with the electrochemical behaviour of the active material. Combined XPS and multinuclear quantitative ⁷Li, ¹H and ¹⁹F NMR indicate a trend for the interphase structure that can be described as a mostly stable inner interphase composed of fluorinated inorganic products while outer lithiated organic species undergo a reversible formation at high potential and dissolution at low potential. Although an irreversible accumulation of interphase occurs, spin–spin relaxation time analysis indicates that interphasial species tend to stack on the top of each other rather than cover the whole active material surface. Moreover, the dissolution/precipitation process seems to prevent a blocking of the electrode surface by resistive species such as LiF.

© 2012 Elsevier B.V. All rights reserved.

1. Introduction

A vast number of research groups has devoted considerable interest to LiFePO₄ since Padhi *et al.* [1] studied the electrochemical properties of polyanionic materials. The initial motives for seeking alternative positive electrode materials to lithium transition metal oxides such as LiCoO₂ [2], Li(Ni,Co,Al)O₂ [3] and LiMn₂O₄ [4] employed in commercial applications were the high cost of raw materials, environmental toxicity as well as the limited thermal stability of some of these compounds. LiFePO₄ displays high theoretical capacity of 170 mA h g⁻¹ with a constant open circuit voltage

of 3.4 V vs Li⁺/Li⁰ [1]. Its orthorhombic olivine-type structure, where oxygen atoms form a slightly distorted hexagonal close packed arrangement ensures a good thermal stability [1,5]. More recently, the low intrinsic electronic conductivity has been bypassed by using synthesis method yielding carbon coated particles [6–10] whereas the reduction of particles size ensures an efficient network and a good accessibility of the active material to lithium ions and electrons and allows achieving high cycling rates retaining specific capacities close to theoretical value [11,12].

Nevertheless, decreasing the particle size typically leads to an increase of the surface area and thus to a subsequent amplification of the parasitic reactions taking place at the interface between the active material surface and the surrounding medium. It is also now realized that all positive electrode materials are reactive with the commonly used electrolyte solutions, developing a complex surface

* Corresponding author. Tel.: +33 2 40 37 39 33; fax: +33 2 40 37 39 95.

E-mail address: nicolas.dupre@cnrs-imn.fr (N. Dupré).

chemistry [13–15]. Electrochemical impedance spectroscopy [16–18] as well as XPS [19–22] and more recently NMR [23–26] have identified the formation of films or deposits of salt-based and solvent-based species (hereafter referred to as the interphase) on the surface of the electrode active material and the electrochemical behaviour of most cathode materials may depend strongly on their surface reactivity towards electrolyte. Attempts to answer these issues are not a straightforward task due to experimental complications including the low amount of surface species that form, the influence of surface chemistry and contaminants in the electrolyte on the composition and structure of the interphase as well as its high sensitivity towards ambient atmosphere [27–30].

Very few studies deal with interphase evolution of LiFePO₄ electrode material upon its operation in a lithium battery as it was considered as chemically inert upon immersion in electrolyte. Concerning the species formed on the surface of grains of active material, Herstedt *et al.* [22] did not observe any organic product such as polycarbonates, polymers or Li alkyl carbonates usually found in the case of oxides. Only products from decomposition of the LiPF₆ electrolyte were detected and no correlation with the electrochemical performance could be made. The decrease of the performance along an increase of the electrode resistance upon storage was however, ascribed by Koltypin *et al.* [31] to a Fe dissolution at elevated temperature. After having noticed the presence of products coming from the decomposition of the electrolyte components on the surface of the active material, it becomes necessary to investigate their formation and evolution along the electrochemical cycling as well as their influence on the battery performance.

The present paper aims at monitoring the evolution of interphase species, using XPS spectroscopy and MAS NMR. Studies are performed on non carbon-coated LiFePO₄ in order to understand the formation and evolution of the active material/LiPF₆ electrolyte interphase. The first electrochemical cycle is investigated in order to understand the processes of reversible formation and dissolution of interphase components as a function of potential. Combined XPS and multinuclear quantitative ⁷Li, ¹H and ¹⁹F NMR indicate a trend for the interphase structure that can be described as a mostly stable inner interphase composed of fluorinated inorganic products while outer lithiated organic species undergo a dissolution process at low potential. The cyclic process of dissolution/precipitation leads nevertheless to an increased mixing of the components of the interphase which can be described after 20 cycles as an organic matrix englobing clusters of LiF and fluorophosphates. Although an irreversible accumulation of interphase occurs, the dissolution/precipitation process seems to prevent a blocking of the electrode surface by resistive species.

2. Experimental

The LiFePO₄ material was synthesized via the solid-state method developed by Yamada *et al.* and described in previous works [28,29]. The iron acetate precursor used in the synthesis is responsible for the presence of carbon residues accounting for approx. 2 wt% and after annealing at 700 °C under Ar/H₂ atmosphere, olivine particles size has been evaluated to 120 nm.

Electrochemical studies were carried out on a Biologic MPG2 using Swagelok-type cells. Electrodes were constituted of 80 wt% of active material, 10 wt% of Ketjenblack carbon and 10 wt% carboxymethylcellulose (CMC). In order to get rid of the binder contributions on ¹H MAS NMR and XPS spectra, a binder-free formulation (90:10) was also used. A slurry of the electrode powder in water was deposited on a 1 cm² aluminium disk and then dried under vacuum at 100 °C for 24 h. The negative electrode was made of a disk of lithium metal, and the electrolyte consisted in

LiPF₆ 1 M in EC:DMC (1:1) solution. Electrodes have been rinsed inside an argon filled glovebox, using few drops of pure DMC just after disassembling the cells in order to get rid of undecomposed dry electrolyte and to ensure the proper detection of the interphase only.

Electrochemical impedance spectroscopy (EIS) measurements (from 200 kHz to 10 mHz) were obtained using a VMP/Z apparatus (Bio-logic, France). A home-made Swagelok-type three electrodes cell was used. The negative electrode was made of a disk of lithium metal. The reference electrode consists of a ring of lithium metal surrounding the working electrode. Measurements have been performed at the end of a 5 h relaxation rest upon discharge down to 2.5 V and upon charge up to 4.5 V for different C/20 galvanostatic cycles at ambient temperature.

X-ray photoelectron spectroscopy (XPS) data were collected after different cycle numbers using a Kratos Ultra Axis spectrometer. The X-ray source is AlK working at 1253.6 eV and the spot size is 0.7 × 0.3 mm. A special air-tied sample holder was used to transfer the samples from the glovebox to the spectrometer, in order to avoid any reaction with ambient atmosphere. Semi-quantitative XPS analysis was performed using pseudo-Voigt function constrained by full width at half-maximum (FWHM) ranges typical of each element. The validity of the analyses was confirmed by an experimental M/O ratio close to the theoretical one for the bare pristine compound. Binding energies were fixed at 0.2 ± eV of the given value.

¹H, ⁷Li, ¹⁹F and ³¹P NMR experiments were carried out at room temperature on a Bruker Avance-500 spectrometer ($B_0 = 11.8$ T, Larmor frequencies $\nu_0(^7\text{Li}) = 194$ MHz, $\nu_0(^{19}\text{F}) = 470$ MHz, $\nu_0(^{31}\text{P}) = 202$ MHz). MAS spectra were obtained by using a Bruker MAS probe with a cylindrical 2.5 mm o.d. zirconia rotor. Spinning frequencies up to 29 kHz were utilized. ⁷Li NMR spectra were acquired by making use of a single pulse sequence coupled with a pre-acquisition time of 4.5 μs allowing the separation of the surface lithium signal from the bulk signal. By this mean, only diamagnetic species on the surface of the paramagnetic active material were observed [23,32,33]. ³¹P NMR spectra were acquired in the same conditions while ¹H and ¹⁹F NMR spectra were acquired using a Hahn echo sequence to discard the significant contribution from the probe signal. All spectra displayed in this work were normalized taking into account the number of scans, the received gain, and the mass of sample. ⁷Li, ¹⁹F and ³¹P integrated intensities were determined by using spectral simulation (Dmfit software [34]).

In previous works, it has been shown that the sidebands manifold width can be correlated to strength of the electron–nucleus dipolar interaction [35]. In particular, the intimacy between lithium in the interphase and paramagnetic electrode grains underneath were probed based on the sidebands manifold width [32,36] as well as through the characteristic T_1^* spin–lattice relaxation time [23,32]. It is also known that the presence of an unpaired electron spin density impacts the broadness of the isotropic resonance as a consequence of a through space nuclear–electron dipolar interaction [35,37,38].

In a further attempt to correlate the material/interphase interaction with the dipolar interaction and its influence on the relaxation times of NMR resonances, the electrode/interphase intimacy (i.e. the strength of the electron–nucleus dipolar interaction) is tentatively discussed through the residual transverse relaxation time of the nucleus under observation, T_{2r} . It can be conveniently estimated from the isotropic resonance linewidth [38,39], avoiding time-consuming additional NMR experiments. In paramagnetic systems, the linewidth can be written as a function of the hyperfine coupling constant A/h , the spin–lattice relaxation time of electrons (T_{1e}) to which the nucleus is coupled and transverse relaxation arising from other effects ($T_{2a,b}$):

$$\text{FWHM} = \frac{1}{T_{2r}} = \frac{1}{T_{2a,b}} + \frac{(A/\hbar)^2 T_{1e}}{8} \quad (1)$$

The terms of Eq. (1) governed by effects other than those induced by the presence of paramagnetic centres is significantly smaller than the paramagnetic contribution [40] and it appears that T_{2r} can be mostly associated with the unpaired electron spin density sitting on the metal centre (T_{1e} and A/\hbar terms) and is therefore depending on the metal electronic spin (i.e. the state of charge, referred to as SOC). Thus, the comparison of NMR signals linewidth (or the T_{2r}) between samples recovered at the same SOC provides an easy estimation of the evolution of electrode/interphase intimacy. T_{2r} values have been estimated using Dmfit software [34]. Accurate proper spin–spin relaxation times (T_2) were also measured by spin echo method and allowed validating the transverse relaxation time estimation as a probe of the electrode/interphase intimacy for sample recovered upon an extended cycling (see *Supplementary data*).

3. Results and discussion

3.1. Characterization of pristine material

The powder morphology of the product is shown in the inset of Fig. 1. All samples display aggregates (5–20 μm) of small grains of approximately 100–200 nm, resulting in a BET specific surface area of $22 \text{ m}^2 \text{ g}^{-1}$. The XRD pattern obtained for the as synthesized LiFePO₄ material is given in *Supplementary data* (Fig. S-1) as well as the results of Rietveld refinement (Table S-1). The diffraction peaks are in full agreement with the LiFePO₄ olivine structure indexed in the orthorhombic *Pnma* space group and no evidence of impurity phases could be observed. The electrochemical performance of this bare LiFePO₄ material was evaluated and the corresponding specific discharge capacity obtained at a C/10 regime is displayed in Fig. 1. As expected, this material exhibits lower performance (158 mA h g⁻¹ over the 20 first cycles) and lower term capacity retention (~6% after 100 cycles) than usually published results [6,10,41,42] due to the absence of conductive/protective carbon. A carbon coating was nevertheless performed and characterized (see *Supplementary data*, Figs. S-1 and S-2) in order to evaluate the electrochemical performance of the material in conditions as close as possible to conventional electrodes. In this case, a specific capacity close to the theoretical one and excellent capacity retention was obtained with 99.8% of the initial capacity after 90 cycles (see *Supplementary data*, Fig. S-3).

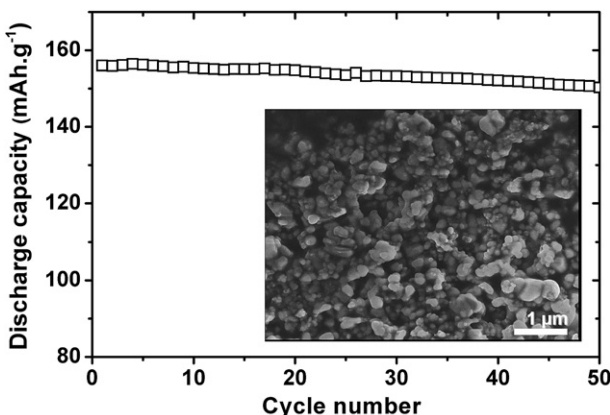


Fig. 1. Discharge capacity at C/10 rate of bare LiFePO₄ material. Inset: SEM picture of the LiFePO₄ raw powder.

3.2. Voltage dependence of the LiFePO₄/electrolyte interphase

The XPS elemental spectra and the deduced elemental percentages obtained along the first electrochemical cycle of LiFePO₄ are displayed in Fig. 2 and Table 1, respectively. The species detected on the surface of the active material are similar to those found on samples soaked or stored in the electrolyte [25] with fluctuations depending on the recovery potential of the sample. Several CO environments are observed between 285.5 and 289.1 eV on the C1s spectra as well as on the O1s spectra at 533.5 eV, with a contribution at 531.5 eV, overlapping with phosphates. These signals, assigned to PEO-type polymers [19,21,43–45] are observed along the first oxidation and first reduction above 3.5 V. They tend to disappear during the second oxidation, from 2 V to 3.5 V.

Fluorine contribution to LiF (685 eV) [21], Li_xPF_y and Li_xPO_yF_z (688 eV) [19,46] increases clearly at the end of the first discharge at 2.0 V. The corresponding percentage decreases slowly during the subsequent oxidation but remains higher than its level during the first cycle. The opposite evolution of organic compounds and inorganic fluorinated species suggests that the two different types of interphase are covering each other although it is not possible to determine which one is closer to the active material and which one constitutes the external part of the interphase.

The covering of the active material can be monitored from Table 1 with the parallel evolutions of the P2p signal corresponding to the LiFePO₄ phosphate group (133.4 eV) and Fe2p. As a general trend, it seems from the evolution of visible iron that the interphase is thicker for high potentials. The antagonist evolutions of visible iron and surface fluorinated species from the one hand, and organic surface species from the other hand, suggest that the organic interphase is mostly covering both the active material and the inorganic part of the interphase. These results are summarized in Fig. 3 and highlight the changes in the composition of the interphase along potential variation encountered by the material during the cycling.

In order to follow the quantitative evolution of surface species, MAS NMR has been performed on the same samples, corresponding to different step (voltage–composition) along the first electrochemical cycle. The corresponding ⁷Li spectra, as well as the resulting quantification of interphasial lithium, are reported in Fig. 4 (see Ref. [33] for details regarding the quantification method).

The interphase appears richer in diamagnetic lithium at high potential, after the oxidation process compared to samples stabilized at 2.7 V and below. As a matter of fact, the ⁷Li NMR signal almost disappears for low potentials. However, lithium containing species are detected by XPS for low potential. Three possible hypotheses would allow explaining this apparent inconsistency by NMR failure to detect the interphase and are discussed below:

First, NMR spectra of paramagnetic materials (here Fe(II) and Fe(III) for LiFePO₄ and FePO₄, respectively) are dominated by extremely large interactions, in particular with unpaired electrons. A strong intimacy between the paramagnetic LiFePO₄ material and the lithiated interphase could yield a strong nucleus–electron dipolar interaction causing a broadening of the NMR signal beyond MAS resolution and mask the corresponding resonances in the reduced state. Indeed, Julien *et al.* [48] showed that the magnetic susceptibility of LiFePO₄ is larger than that of FePO₄. However, in this hypothetic case, the ⁷Li NMR signal of remaining detected lithium is expected to display an extremely wide sidebands manifold. This is not the case here and the width of the sidebands manifold for reduced samples, spanning on up to 1000 ppm, is smaller than what can be observed in the case of the interphase detected on the surface of the oxidized samples (2000 ppm, see Fig. 4a) and of

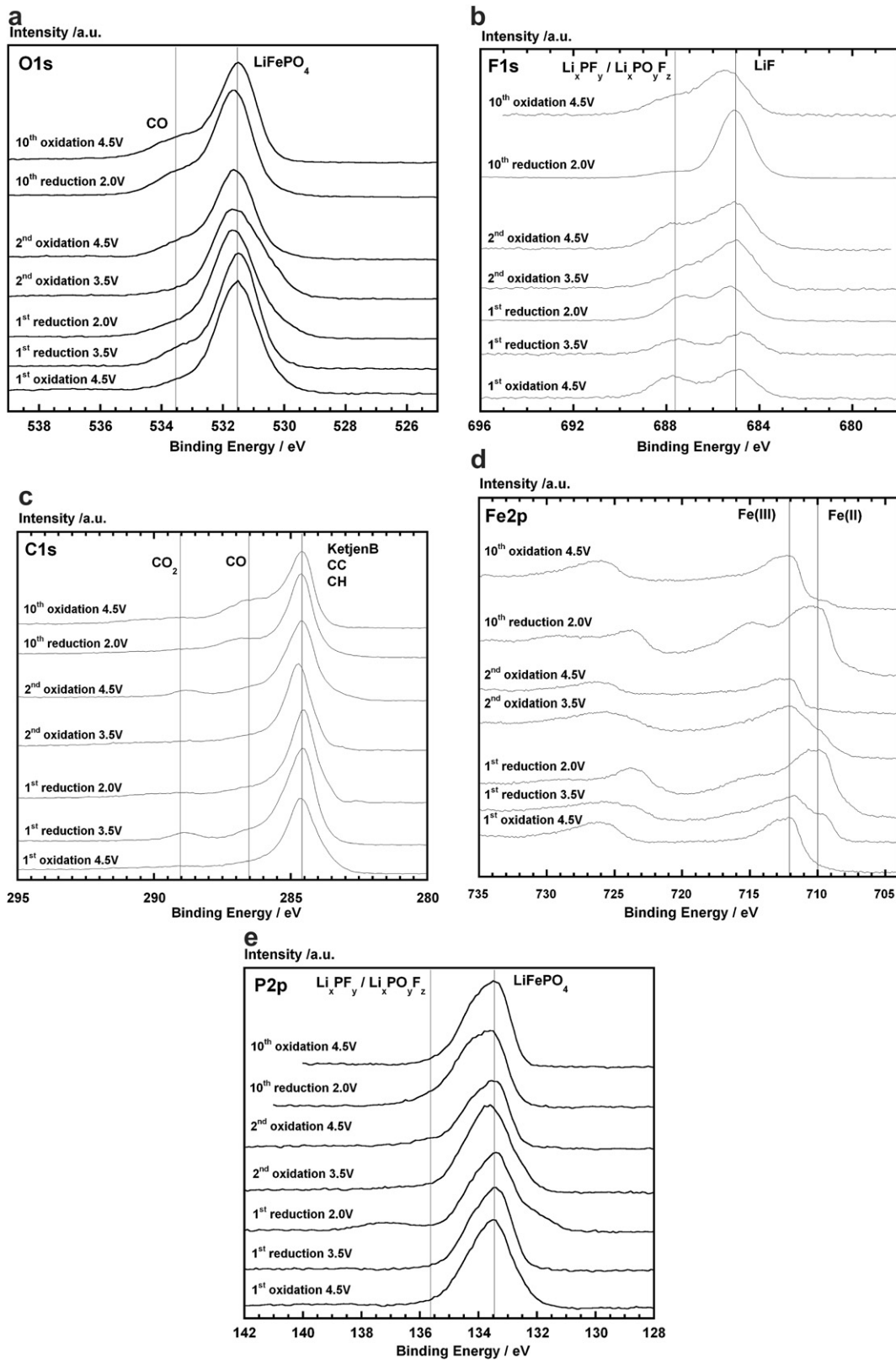


Fig. 2. (a) F1s, (b) P2p, (c) C1s, (d) O1s and (e) Fe2p XPS spectra for binder-free electrodes of LiFePO₄ along the first two and the 10th electrochemical cycles (C/10) in LiPF₆ 1 M EC:DMC (1:1).

Table 1

Quantitative evolution of elemental percentages obtained from the analysis of XPS spectra for binder-free electrodes of LiFePO₄ during the first electrochemical cycle (C/10) in LiPF₆ 1 M EC:DMC (1:1) and for the 10th cycle. Binding energies are constrained at ± 0.2 eV. Concerning the iron signal, binding energies corresponding to Fe2p_{3/2} peaks are given in the table but the quantification has been performed on the Fe2p_{1/2} peaks due to the possible overlapping with a fluorine satellite [47]. Detected element within a chemical group is given in bold.

Binding energy	4.5 V ox1	4.1 V red1	3.5 V red1	2.7 V red1	2 V red1	2.7 V ox2	3.5 V ox2	4.1 V ox2	4.5 V ox2	4.5 V ox10	2.0 V red10
C sp ²	284.6 eV	46%	41%	40%	39%	36%	37%	32%	36%	43%	27%
CC–CH	285.5 eV	2%	8.5%	10.5%	10%	4.5%	4%	12%	7%	5.5%	7%
CO	286.5 eV	4.5%	4.5%	4.5%	4.5%	2.5%	2.5%	1.5%	4.5%	4.5%	7%
CO	287.7 eV	1.5%	1.5%	1.5%	1.5%	1%	0.5%	0.5%	2%	1.5%	4%
CO ₂	289.1 eV	2%	3.5%	4%	4%	1.5%	1%	0.5%	3%	4%	0.5%
PO ₄	531.5 eV	31.5%	27.5%	25.5%	24%	29%	29%	33%	26%	23.5%	32%
CO–OH	533.5 eV	1%	3.5%	4%	5%	2.5%	3.5%	1%	5%	3.5%	7%
LiF	685.1 eV	3%	3%	2%	3%	8.5%	7%	6.5%	4%	5.5%	5%
Li _x PO _y F _z	687.6 eV	2%	1.5%	1%	1.5%	6%	4%	2.5%	5%	3%	2%
PO ₄	133.4 eV	3.5%	3%	4%	4.5%	5%	5%	6%	4%	3.5%	4%
PO	135.7 eV	0%	0%	0%	0.5%	0%	1.5%	0.5%	1%	0.5%	1%
PF	137 eV	0%	0%	0%	0%	0.5%	0%	0%	0%	0%	0%
Fe(II)	709.9 eV	0%	0%	1.5%	2%	4%	3.5%	2%	0%	0%	0.2%
Fe(III)	712.0 eV	3%	3%	1.5%	0.5%	0%	1.5%	2%	2.5%	2%	2.8%

nickel manganese oxides (up to 3000 ppm) [23]. Hence a too strong nuclear-electronic dipolar interaction cannot be considered as impeding the detection of interphasial diamagnetic species at the surface of LiFePO₄ compared to FePO₄.

- Second, the NMR signal fading could also be a consequence of the dissolution of iron in the electrolyte, some of it being trapped in the interphase, leading to a close mixing with the interphasial species. However in this case, the electron-nuclear dipolar interaction would then remain extremely strong upon further cycling, independently from the SOC. As a result, due to proximity of Fe trapped in the interphase, estimated

interphasial Li T_{2r} should remain short after iron dissolution instead of recovering its value from the previous oxidation (Fig. 4b). This second hypothesis can therefore also be ruled out.

- Third, following the evolution of ⁷Li NMR and XPS signals, the lithium containing species detected by NMR undergo a process of dissolution at low potentials and precipitation at high potentials that can be seen as a reversible “breathing” process. As it has been seen for other materials [24,26], the interphase formed appears as a potential dependent dynamic system. Finally the observed T_{2r(Li)} evolution is the result of both SOC variations and the evolving distribution of lithiated species within the interphase, varying along this reversible “breathing” process. The fact that the amount of lithium detected by XPS does not decrease along this dissolution process can be explained by the extreme surface sensitivity of the technique: in spite of the dissolution of a major part of interphase present at high potential, the lithiated species remaining at low potential can still account for similar elemental percentage at the scale of the 5 nm depth typically probed by XPS.

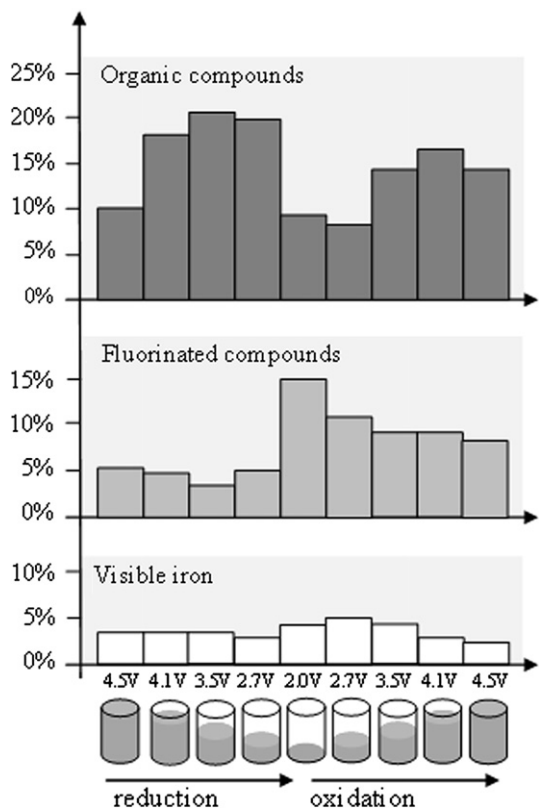


Fig. 3. Evolution of the amount of carbonaceous (corresponding to C1s peaks between 285.5 and 289.1 eV), fluorinated species and iron along the first electrochemical cycle for binder-free electrodes of LiFePO₄.

¹H MAS NMR (Fig. 5, left) analysis allows confirming the correlation between the surface organic species and the lithium signal detected by ⁷Li MAS NMR. The detected protons could be separated into two kinds of contributions. The signal observed, centred at -4 ppm, gives rise to the spinning sidebands denoted by the asterisks, sign of a strong interaction with the paramagnetic electrode material. The variation of both intensity and sidebands manifold span follow the evolution observed previously for ⁷Li NMR signal, with an extremely broad sidebands manifold at high voltage. A second contribution, most probably coming from a possible residual signal from the probe, without any sideband was also observed. This contribution, very difficult to estimate, was therefore accounted as purely diamagnetic, with no interaction with the paramagnetic active material and has not been considered further in the present work.

¹⁹F MAS NMR maybe provides more unambiguous information, insofar LiF signal at -204 ppm can clearly be separated from that of fluorophosphates arising around -77 ppm and -85 ppm for R–PO₃F and R–PO₂F₂, respectively (Fig. 5, right) [49]. Rather than the net decrease observed in the amount of lithiated or protonated species, the electrochemical reduction is mostly accompanied by a significant broadening of the ¹⁹F NMR signals. The different variations observed on ⁷Li and ¹⁹F signals (see Fig. 6) suggest that ⁷Li NMR mainly probes the evolution of non fluorinated species.

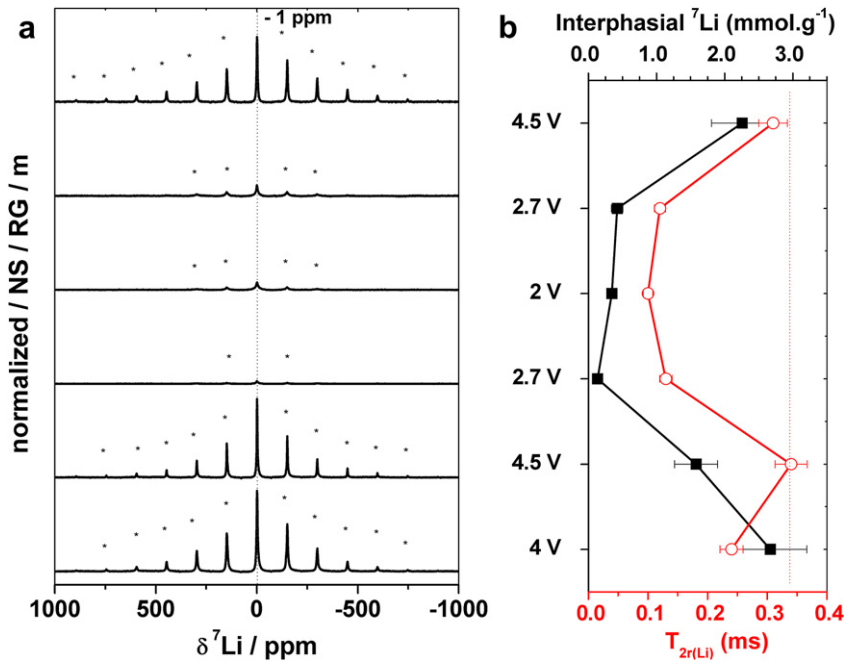


Fig. 4. (a) Normalized ${}^7\text{Li}$ NMR spectra for binder-free electrodes of LiFePO_4 along the first electrochemical cycle at a C/20 regime in $\text{LiPF}_6/\text{EC:DMC}$. Asterisks denote spinning sidebands. (b) The amounts of interphasial lithium deduced from integrated intensities, as well as T_{2r} s estimated by the signal width are reported on the right.

The amount of fluorine nuclei involved in the interphase does not vary significantly upon potential variation and only a line broadening due to the change of the oxidation state of iron, altering the nucleus–electron dipolar interaction, is observed. Due to this signal broadening, it is not possible, at this stage, to completely rule out the presence of remaining LiPF_6 , which signal would arise at -70 ppm. Complementary ${}^{31}\text{P}$ MAS NMR (see **Supplementary data**, Fig. S-4), performed at the end of charge and discharge, completes the multinuclear investigation as the qualitative assignment of NMR shifts is straightforward. Should excess electrolyte salt be present in our samples, the corresponding isotropic ${}^{31}\text{P}$ NMR signal for LiPF_6 would be observed at -145 ppm, far away from that of $\text{R}-\text{PO}_3\text{F}$ and $\text{R}-\text{PO}_2\text{F}_2$, at -10 ppm and -22 ppm,

respectively [49]. The experimental observation of a broad signal centred around -17.5 ppm is assigned here to a mixture of these two types of fluorophosphates.

Aiming at summarizing all the experimental results discussed above, Fig. 6 contains the NMR quantifications obtained along the first electrochemical cycle. ${}^{31}\text{P}$ MAS NMR results are here reported in the light of the detected amounts of fluorine in fluorophosphates. The F/P ratio stays mostly quite close to 2 and confirms that the detected species correspond rather to $\text{R}-\text{PO}_2\text{F}_2$ (F/P = 2) or a mixture with $\text{R}-\text{PO}_3\text{F}$ (F/P = 1) than LiPF_6 (F/P = 6), as suggested by the assignments made from the NMR shifts.

Free from the detrimental screening effect faced with XPS, multinuclear NMR quantification indicates that the amounts of LiF

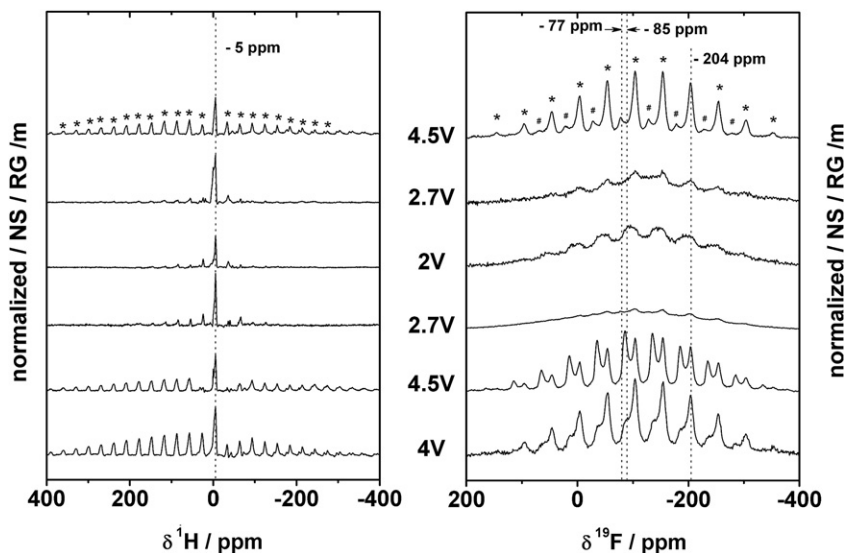


Fig. 5. ${}^1\text{H}$ and ${}^{19}\text{F}$ MAS NMR normalized spectra for binder-free electrodes of LiFePO_4 along the first electrochemical cycle at a C/20 regime in $\text{LiPF}_6/\text{EC:DMC}$.

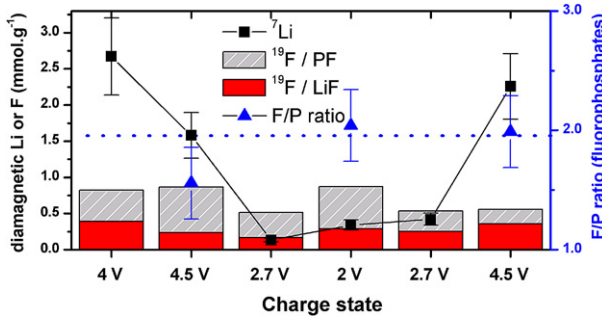


Fig. 6. NMR quantification results for binder-free electrodes of LiFePO_4 along the first electrochemical cycle at a C/20 regime in $\text{LiPF}_6/\text{EC:DMC}$.

and fluorophosphates do not vary significantly along the first electrochemical cycle. Moreover, it appears that the evolution of interphase species observed by NMR upon potential variations mostly concerns “fluorine-free” lithiated species such as Li-alkyl carbonates. This conclusion is in full agreement with XPS results, and with the idea of a dynamic organic interphase mostly covering both the active material and the inorganic part of the interphase. Based on purely macroscopic spectroanalytical techniques, a 3D, dynamic model of the LiFePO_4 /electrolyte interphase can be pictured with an inner part of the interphase mainly comprised of stable LiF and fluorophosphates and an outer part mostly composed of lithiated organic species, under the form of a solid polymer layer (SPL) subject to dissolution/precipitation processes along potential variations.

The interphase formed during the first electrochemical cycle of a Li-ion battery behaves as a dynamic system as a function of the potential. It can be expected to play a significant role on the battery performance for a greater number of cycles. Indeed, a critical point is to ensure the passivation of both reactive electrode surfaces in order to limit (or ideally to stop) lithium consumption in the interphases and the resulting capacity fading along prolonged cycling. The following section focuses on the twenty first electrochemical cycles of the Li/LiPF_6 , $\text{EC:DMC}/\text{LiFePO}_4$ system.

3.3. Evolution of the interphase over 20 cycles

Electrochemical impedance spectroscopy (EIS) measurements were performed at the end of the 1st, 5th and 20th cycles, after a 5 h rest, as shown from the Nyquist diagrams in Fig. 7. The flat shape of the EIS loop is in full accordance with a SPL model of the interphase [50]. As previously demonstrated, the flattened semi-circle can be assigned to charge transfer phenomena [25]. No additional semi-circle can be observed at higher frequencies, therefore suggesting that the interphase grown on LiFePO_4 does not behave as a strictly resistive film (or that it is not covering homogeneously the surface). Noteworthy, the impedance measured along cycling hardly increases, and the characteristic frequency sees no evolution either, indicating that no interphasial phenomenon impeding the charge transfer appears. Hence, the evolution of the LiFePO_4 /electrolyte interphase along cycling, if any, does not induce any conductivity limitation to the system, in agreement with previously reported literature [19,22].

Complementary XPS measurements after 10 cycles at the end of charge (4.5 V) and discharge (2 V) were performed in order to sample the interphase extreme surface composition along the electrochemical cycling. The corresponding spectra and quantitative measurements are displayed in Fig. 2 and Table 1, respectively. The same species are found on the surface of the active material compared to the early stages of the cycling. LiF is present (F1s at

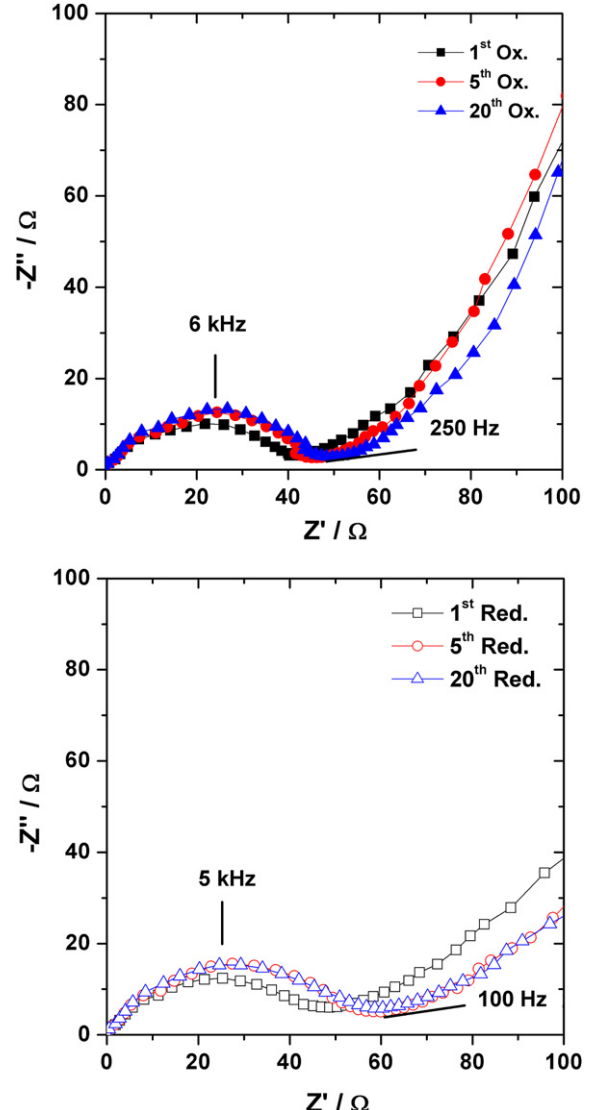


Fig. 7. Nyquist plots of EIS performed on LiFePO_4 electrodes at the end of the 1st, 5th and 20th charges (closed symbols, top) and discharges (open symbols, bottom) at a C/20 rate.

685 eV) as well as other fluorinated species such as Li_xPF_y and $\text{Li}_x\text{PO}_y\text{F}_z$ (F1s at 688 eV, P2p3/2 at 135 eV) in slightly lower amounts, as deduced from data shown in Table 1. Several CO groups are present on the carbon spectrum (C1s in the 286–290 eV range) as well as on the oxygen spectrum (O1s at 533.5 and 531.5 eV). The detected amount of LiF depends strongly on the potential and as a matter of fact, a factor 4 can be calculated between the oxidized and reduced state. These observations are consistent with the behaviour of the system during the first cycle, the inorganic part of the interphase being covered by organic species at the end of oxidation. However, there seems to be an accumulation of fluorinated species for an extended cycling with a clear increase of surface fluorine from 14.5% (8.5% and 6% for LiF and fluorophosphates, respectively) to 26% (22% and 4% for LiF and fluorophosphates, respectively) from the first to the 10th cycle.

Concerning the carbon signals, the sum of the percentages corresponding to the 285.5–290 eV range for the first cycle (9.5% and 15.5% in reduced and oxidized states respectively) and the 10th cycle (10.5% and 18.5% in reduced and oxidized states respectively)

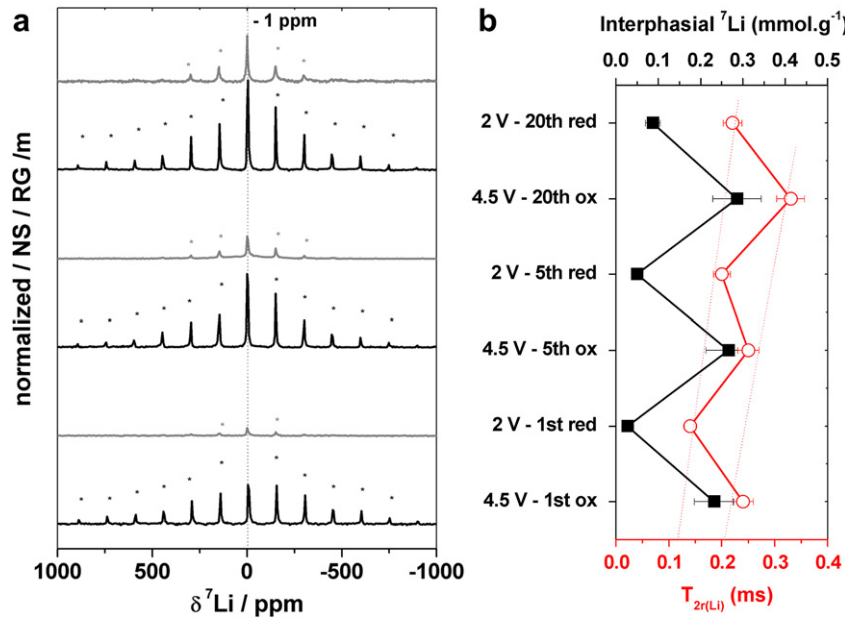


Fig. 8. (a) Normalized ${}^7\text{Li}$ NMR spectra for LiFePO_4 electrodes at the end of the 1st, 5th and 20th charges and discharges at a C/20 rate in $\text{LiPF}_6/\text{EC:DMC}$. (b) Amounts of interphasial lithium deduced from integrated intensities, as well as T_{2r} s estimated from the signal width are reported on the right.

are nevertheless, quite similar. It seems then, that, unlike fluorinated species, only a small accumulation of organic species occurs along the electrochemical cycling, with a stable dissolution/precipitation phenomenon along the reduction/oxidation process.

In order to monitor the evolution of amounts of species as well as their interaction with the surface of active material, ${}^7\text{Li}$ and ${}^{19}\text{F}$ MAS NMR have been performed on positive electrodes stopped after 1, 5 and 20 cycles at the end of charge and end of discharge. The ${}^7\text{Li}$ NMR spectra are presented in Fig. 8 together with the resulting quantification plot. The interphase dynamics revealed during the first electrochemical cycle is confirmed by these additional experiments. Indeed, the process of dissolution at low potentials and precipitation at high potentials of lithiated species appears reversible, although a slight accumulation of both lithiated and fluorinated species is observed between the 1st, 5th and 20th charges and discharges, in agreement with XPS measurements at the 10th cycle.

Considering points taken at the same SOC, T_{2r} increase along cycling (Fig. 8b) suggests the weakening of the overall nuclear-electronic dipolar interaction, hence an average weakening of the electrode/interphase intimacy. As explained in Ref. [23], this observation can imply either a thicker interphase or a more loosely attached one. The increase observed in the amounts of interphasial

lithium supports the first hypothesis, while the repeated dissolution/precipitation process allows explaining the second. Both are probably intervening here.

Results from ${}^{19}\text{F}$ MAS NMR appear in Fig. 9, under the form of a quantification diagram. At the scale of the twenty first cycles, it appears that the amounts of fluorinated species also evolve along cycling. These results suggest in particular an increasing mixing of the different components of the interphase along the electrochemical cycling. In these conditions, it does not seem unlikely that the dissolution of the SPL matrix would result in the detachment of less soluble inorganic species upon discharge. During the subsequent charge, those fluorinated salts occur to be trapped again in the reformed SPL. Such close mixing of interphasial species as well as chemical inhomogeneities within the interphase have been in particular revealed by EELS measurements in the case of other electrode materials [33].

The accumulation observed between the 1st, 5th and 20th charges and discharges of LiF and fluorophosphates in the LiFePO_4 /electrolyte interphase may seem inconsistent with the unchanging impedance. However, these combined results, again, support the conception of an interphase in decreasing intimacy with the active material and/or porous enough to allow charge transfer between the electrode and liquid electrolyte. Preventing the blocking of the electrode surface by salt decomposition products, the repeated

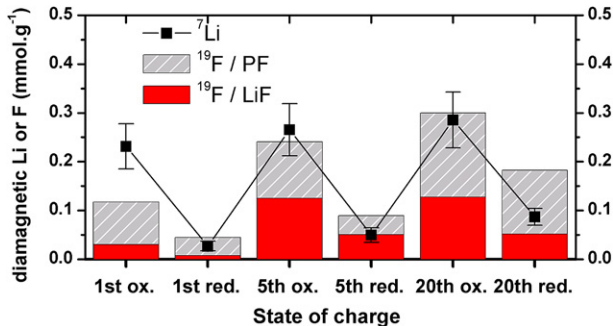


Fig. 9. NMR quantification results for LiFePO_4 electrodes at the end of the 1st, 5th and 20th charges and discharges at a C/20 rate in $\text{LiPF}_6/\text{EC:DMC}$.

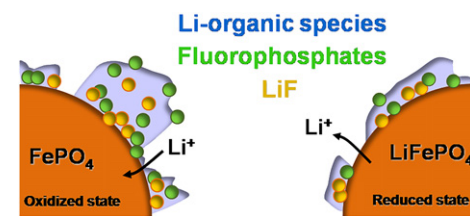


Fig. 10. Schematic view of the interphase pictured on LiFePO_4 at the charged and discharged states along cycling in conventional LiPF_6 1 M in EC:DMC (1:1) electrolyte. The higher amount of lithiated organic species does not seem to hamper the interfacial charge transfer, for additional interphasial species tend to stack on the top of the preexisting interphase.

dissolution/precipitation process of the organic component of the interphase is therefore significantly beneficial to the electrochemical performance of the positive electrode.

4. Conclusions

Widely considered as chemically inert towards the electrolyte, LiFePO₄ actually exhibits a complex, dynamic interaction with classical LiPF₆/EC:DMC electrolyte solution. As tentatively represented in Fig. 10, the present study reveals that:

- Solvents are degraded on LiFePO₄ surface at high potentials, and their decomposition products form a solid polymer layer type interphase that subsequently dissolves at lower potentials.
- Less voltage-sensitive salt decomposition products such as LiF, Li_xPF_y and Li_xPO_yF_z compounds are trapped in this SPL. Although a significant amount departs along the organic matrix dissolution, the interphase observed at low potential is therefore richer in fluorinated compounds.
- The net accumulation of interphasial species is balanced by a looser attachment of this SPL-type interphase to LiFePO₄ surface, and also by the emphasis of topological inhomogeneities resulting in an enhanced SPL porosity. New interphasial species stack on the top of the existing interphase rather than further cover the active material surface, hence preventing the blocking of charge transfer between the electrolyte and the active material.

Nevertheless, the benefit of such interphase dynamics should not eclipse the overall accumulation of lithiated decomposition products at the positive electrode surface. The experiments conducted here do not allow identifying the source of those lithiated species; further analyses performed in a Li-ion configuration would be necessary to discriminate a “cross-talk” between the negative and the positive electrode interphases from detrimental faradic lithium consumption. The answer to this last question would enable for instance choosing appropriate additive(s), either to facilitate the shuttle of interphasial species between the two electrodes or to strictly passivate LiFePO₄ surface.

Appendix A. Supplementary data

Supplementary data associated with this article can be found in the online version, at <http://dx.doi.org/10.1016/j.jpowsour.2012.08.099>.

References

- [1] A.K. Padhi, K.S. Nanjundaswamy, J.B. Goodenough, *J. Electrochem. Soc.* 144 (1997) 1188.
- [2] L. Li, W.H. Meyer, G. Wegner, M.W. Mehrens, *Adv. Mater.* 17 (2005) 984.
- [3] M. Nagata, A. Sarawat, H. Nakahara, H. Yumoto, D.M. Skinlo, K. Takeya, H. Tsukamoto, *J. Power Sources* 146 (2005) 762.
- [4] L. Tao, Q. Weihua, Z. Hailei, L. Jingjing, *Rare Metals* 27 (2007) 280.
- [5] V.A. Streltsov, E.L. Belokoneva, V.G. Tsirelson, N.K. Hansen, *Acta Crystallogr. B49* (1993) 147.
- [6] H. Huang, S.C. Yin, L.F. Nazar, *Electrochem. Solid-State Lett.* 4 (10) (2001) A170.
- [7] C.H. Mi, G.S. Cao, X.B. Zhao, *Mater. Lett.* 59 (1) (2005) 127.
- [8] N.J. Yun, H.W. Ha, K.H. Jeong, H.Y. Park, K. Kim, *J. Power Sources* 160 (2) (2006) 1361.
- [9] R. Dominko, M. Bele, M. Gaberscek, M. Remskar, D. Hanel, S. Pejovnik, J. Jamnik, *J. Electrochem. Soc.* 152 (3) (2005) A607.
- [10] S.Y. Chung, J.T. Bloking, Y.M. Chiang, *Nat. Mater.* 1 (2) (2002) 123.
- [11] C. Delacourt, L. Laffont, R. Bouchet, C. Wurm, J.B. Leriche, M. Morcrette, J.M. Tarascon, C. Masquelier, *J. Electrochem. Soc.* 152 (5) (2005) A913.
- [12] A. Yamada, S.C. Chung, K. Hinokuma, *J. Electrochem. Soc.* 148 (3) (2001) A224.
- [13] D. Aurbach, B. Markovsky, M.D. Levi, E. Levi, A. Schechter, M. Moshkovich, Y. Cohen, *J. Power Sources* 95 (1999) 81.
- [14] D. Aurbach, B. Markovsky, G. Salitra, E. Markevich, Y. Talyossef, M. Koltypin, L. Nazar, B. Ellis, D. Kovacheva, *J. Power Sources* 165 (2) (2007) 491.
- [15] M.G. Thomas, P.G. Bruce, J.B. Goodenough, *J. Electrochem. Soc.* 132 (1985) 1521.
- [16] M.D. Levi, G. Salitra, B. Markovsky, H. Teller, D. Aurbach, U. Heider, L. Heider, *J. Electrochem. Soc.* 146 (1999) 1276.
- [17] C.H. Chen, J. Liu, K. Amine, *J. Power Sources* 96 (2001) 321.
- [18] D. Aurbach, B. Markovsky, Y. Talyossef, G. Salitra, H.J. Kim, S. Choi, *J. Power Sources* 162 (2) (2006) 780.
- [19] K. Edström, T. Gustafsson, J.O. Thomas, *Electrochim. Acta* 50 (2004) 397.
- [20] T. Eriksson, A.M. Andersson, C. Gejke, T. Gustafsson, J.O. Thomas, *Langmuir* 18 (2002) 3609.
- [21] A. Nyten, M. Stjerndahl, H. Rensmo, H. Siegbahn, M. Armand, T. Gustafsson, K. Edstrom, J.O. Thomas, *J. Mater. Chem.* 16 (2006) 3483.
- [22] M. Herstedt, M. Stjerndahl, A. Nyten, T. Gustafsson, H. Rensmo, H. Siegbahn, N. Ravet, M. Armand, J.O. Thomas, K. Edström, *Electrochim. Solid-state Lett.* 6 (2003) A202.
- [23] N. Dupré, J.F. Martin, D. Guyomard, A. Yamada, R. Kanno, *J. Mater. Chem.* 18 (2008) 4266.
- [24] N. Dupré, J.F. Martin, J. Oliveri, D. Guyomard, A. Yamada, R. Kanno, *Electrochim. Commun.* 10 (12) (2008) 1897.
- [25] N. Dupré, J.F. Martin, J. Degryse, V. Fernandez, P. Soudan, D. Guyomard, *J. Power Sources* 195 (21) (2010) 7415.
- [26] N. Dupré, J.F. Martin, J. Oliveri, P. Soudan, D. Guyomard, A. Yamada, R. Kanno, *J. Power Sources* 196 (10) (2011) 4791.
- [27] J.F. Martin, A. Yamada, G. Kobayashi, S. Nishimura, R. Kanno, D. Guyomard, N. Dupré, *Electrochim. Solid-State Lett.* 11 (1) (2007) A12.
- [28] M. Cuisinier, J.F. Martin, N. Dupré, A. Yamada, R. Kanno, D. Guyomard, *Electrochim. Commun.* 12 (2) (2010) 238.
- [29] J.F. Martin, M. Cuisinier, N. Dupré, A. Yamada, R. Kanno, D. Guyomard, *J. Power Sources* 196 (2011) 2155.
- [30] M. Cuisinier, J.F. Martin, N. Dupré, R. Kanno, D. Guyomard, *J. Mater. Chem.* 21 (2011) 18575.
- [31] M. Koltypin, D. Aurbach, L. Nazar, B. Ellis, *J. Power Sources* 174 (2) (2007) 1241.
- [32] M. Ménétrier, C. Vaysse, L. Croguennec, C. Delmas, C. Jordy, F. Bonhomme, P. Biensan, *Electrochim. Solid-State Lett.* 7 (6) (2004) A140.
- [33] M. Cuisinier, J.F. Martin, P. Moreau, T. Epicier, R. Kanno, D. Guyomard, N. Dupré, *Solid State Nucl. Magn. Reson.* 42 (2012) 51.
- [34] D. Massiot, <http://nmr.chemt.cnrs-orleans.fr/dmfit/>.
- [35] C.P. Grey, N. Dupré, *Chem. Rev.* 104 (2004) 4493.
- [36] N. Dupré, J.F. Martin, J. Oliveri, P. Soudan, D. Guyomard, A. Yamada, R. Kanno, *J. Electrochem. Soc.* 156 (6) (2009) C180.
- [37] A. Nayem, J.P. Yesinowski, *J. Chem. Phys.* 89 (1988) 4600.
- [38] L.J.M. Davis, I. Heimmaa, B.L. Ellis, L.F. Nazar, G.R. Goward, *Phys. Chem. Chem. Phys.* 13 (2011) 5171.
- [39] T.J. Swift, in: G.N. La Mar, W. Horrocks Jr., R.H. Holm (Eds.), *NMR of Paramagnetic Materials*, Academic Press, New York, 1973, p. 53.
- [40] F.H. Kohler, in: J.S. Miller, M. Drillon (Eds.), *Magnetism: Molecules to Materials*, vol. 1, Wiley-VCH, New York, 2001, p. 386.
- [41] Z.H. Chen, J.R. Dahn, *J. Electrochem. Soc.* 149 (2002) A1184.
- [42] D.H. Kim, J. Kim, *Electrochim. Solid-State Lett.* 9 (2006) A439.
- [43] V. Eshkenazi, E. Peled, L. Burstein, D. Golodnitsky, *Solid State Ionics* 170 (2004) 83.
- [44] R. Dedryvère, S. Laruelle, S. Gruegeon, L. Gireaud, J.M. Tarascon, D. Gonbeau, *J. Electrochem. Soc.* 152 (2005) A689.
- [45] D. Aurbach, I. Weissman, A. Schechter, *Langmuir* 12 (1996) 3991.
- [46] S.H. Kang, D.P. Abraham, A. Xiao, B.L. Lucht, *J. Power Sources* 175 (2008) 526.
- [47] M. Scrocco, *Phys. Rev. B* 32 (1985) 1306.
- [48] A. Ait-Salah, J. Dodd, A. Mauger, R. Yazami, F. Gendron, C.M. Julien, Z. Anorg. Allg. Chem. 632 (2006) 1598.
- [49] A.V. Plakhotnyk, L. Ernst, R. Schmutzler, *J. Fluorine Chem.* 126 (2005) 27.
- [50] J.G. Thevenin, R.H. Muller, *J. Electrochem. Soc.* 134 (1987) 273.